

## Effect of welding sequence on residual stress in thin-walled octagonal pipe–plate structure

Ding-fa FU<sup>1</sup>, Chang-qing ZHOU<sup>1</sup>, Can LI<sup>1</sup>, Guan WANG<sup>2</sup>, Luo-xing LI<sup>2</sup>

1. College of Materials Science and Engineering, Hunan University, Changsha 410082, China;

2. State Key Laboratory of Advanced Design and Manufacture for Vehicle Body, Hunan University, Changsha 410082, China

Received 5 March 2013; accepted 15 July 2013

**Abstract:** A three-dimensional finite element approach based on ABAQUS code was developed to investigate the effect of welding sequence on welding residual stress distribution in a thin-walled 6061 aluminum alloy structure. To obtain sound numerical results, the thermo-mechanical behaviour was simulated using a direct-coupled formulation. Nine different simulation sequences were carried out by single-pass TIG welding of an octagonal pipe–plate joint, and the distributions of longitudinal and transverse residual stresses both on the outer and inner surfaces of the pipe were analyzed. The results suggest that the final residual stresses in the weld and its vicinity are not affected by the initial residual stresses of the structure. Selecting a suitable welding sequence can reduce the final residual stress in an octagonal pipe–plate joint.

**Key words:** residual stress; welding sequence; pipe–plate joint; single-pass welding; initial residual stress

### 1 Introduction

The residual stress in welded structures mainly results from the non-uniform expansion and contraction of the weld and the base material in the vicinity, due to a non-uniform temperature field during welding. High residual stress within and near the weld zone may lead to brittle fracture, reduce the fatigue life and promote stress corrosion cracking during service. Therefore, welding residual stress must be controlled to insure the integrity of the structures.

The method of numerical simulation is widely used to predict welding residual stress and distortion. LIU et al [1] presented a pass-by-pass finite element simulation to investigate the residual stress in narrow gap multipass welding of pipes with 73 weld passes, and the simulation results were validated by experimental data. SCHENK et al [2] employed a numerical case to study the influence of clamping on welding residual stress and distortion and the results showed that the final residual stresses and distortions strongly depended on the clamping conditions.

To reduce residual stress in 316L stainless steel welding joint, JIANG et al [3] used finite element method to study the effect of heat sink on residual stress and it was found that the heat sink technology could reduce by 20% of the peak longitudinal stress. The above researches are not capable of predicting the effect of welding sequences and weld start/stop locations [4–8].

CHANG and LEE [9] investigated the influence of the welding sequence on residual stress distribution in pipe welding. They employed six different welding sequences in the simulation and the results showed that the residual stresses within and near the weld deposit were affected by the welding sequences. Furthermore, they found the benefits arising from the change of the residual stresses in the weld and its vicinity were offset by the potential drawback of the several start/stop locations. SATTARI-FAR and JAVADI [10] studied the influence of welding sequences on welding distortions in pipe–pipe joint based on single-pass TIG welding with V-joint geometry. The simulation results were compared with experimental data and the results revealed that selecting a suitable welding sequence could substantially

**Foundation item:** Project (61075005) supported by the Fund of State Key Laboratory of Advanced Design and Manufacture for Vehicle Body in Hunan University, China; Project (09JJ1007) supported by Preeminent Youth Fund of Hunan Province, China; Project (51075132) supported by the National Natural Science Foundation of China

**Corresponding author:** Ding-fa FU; Tel: +86-13873151148; E-mail: [hunu\\_fudingfa@163.com](mailto:hunu_fudingfa@163.com)

DOI: 10.1016/S1003-6326(14)63108-3

decrease the magnitude of welding distortions.

From the above analysis we can draw that most researches were focused on the influence of welding sequence on flat plate or round pipe structure, but few researches [11] were done on polygonal pipes. This work presents a 3D finite element model to investigate the influence of nine different welding sequences in an octagonal pipe–plate structure using the FE code ABAQUS [12]. In the simulation, the DFLUX user subroutine compiled by FORTRAN program is employed to realize a moving welding arc which is presented in ABAQUS as the heat fluxes [13].

## 2 Analysis model

A mock-up was fabricated to confirm the accuracy of the simulation shown in Fig. 1, which is composed of a regular octagonal pipe with a smaller regular octagonal pipe inside and a bottom plate. The height, outside wall thickness, interior wall thickness and thickness of stiffeners of the pipes are 200 mm, 2.37 mm, 2.25 mm and 1.5 mm, respectively. The dimensions of the bottom plate are 173 mm×138 mm×5 mm. The welding start location and the front, back, left and right sections are

depicted in Fig. 1. The material of the whole structure is 6061-T6 aluminum and the solder is supposed to be of the same material with the base metal.

### 2.1 Finite element model

The FE mesh is shown in Fig. 2 and the dimensions of the FE model are the same as that used in the experiment. Dense mesh is applied in the welding seam and the angularity area while coarse mesh is for the rest of the structure to reduce the computational cost. Brick elements with eight nodes and quadratic elements with four nodes are used in the model. The FE mesh contains a total of 76602 nodes with associated 22729 elements.

### 2.2 Material model

Material properties play a significant role in welding simulation due to the fact that they have important effects on the accuracy of the results. The properties of the materials change when suffering from a thermal cycle, so the temperature-dependent physical properties and mechanical properties are considered in this work. Because of the lack of material data at elevated temperatures, the detailed material model for the material described is not available. Table 1 presents

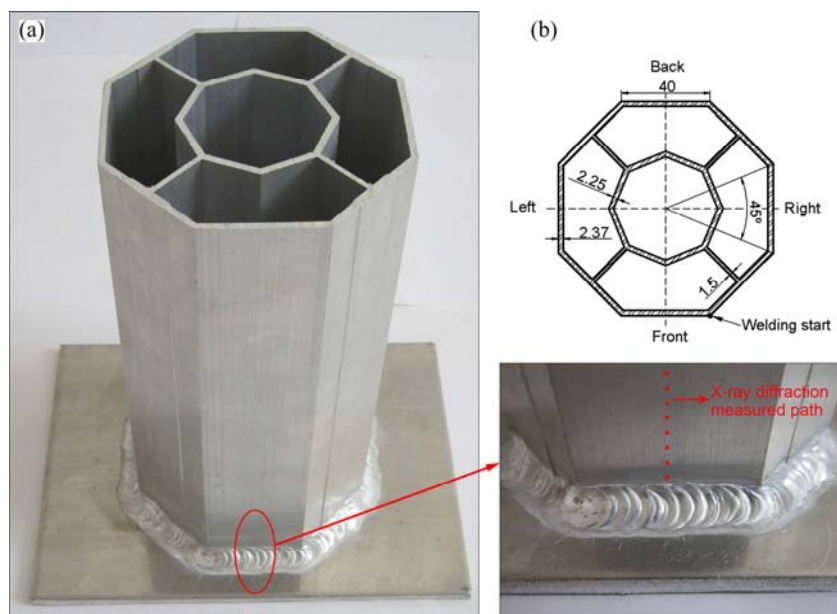


**Fig. 1** Configuration of welding structure (a) and X-ray diffraction measured path (b) (unit: mm)

**Table 1** Temperature-dependent properties for 6061-T6 aluminum alloy

Temperature/ °C	Heat conductivity/ (W·m <sup>-1</sup> ·°C <sup>-1</sup> )	Specific heat capacity/ (J·kg <sup>-1</sup> ·°C <sup>-1</sup> )	Density/ (kg·m <sup>-3</sup> )	Expansion coefficient/10 <sup>-6</sup> °C <sup>-1</sup>	Elastic modulus/ GPa	Yield stress/ MPa
20	162	945	2700	23.45	68.54	274.4
93.3	177	978	2685	24.61	66.19	264.6
204.4	192	1028	2657	26.6	59.16	218.6
260	201	1052	2657	27.56	53.99	159.7
371	217	1104	2630	29.57	40.34	36.84
482.2	226	1136	2602	31.71	20.2	10.49

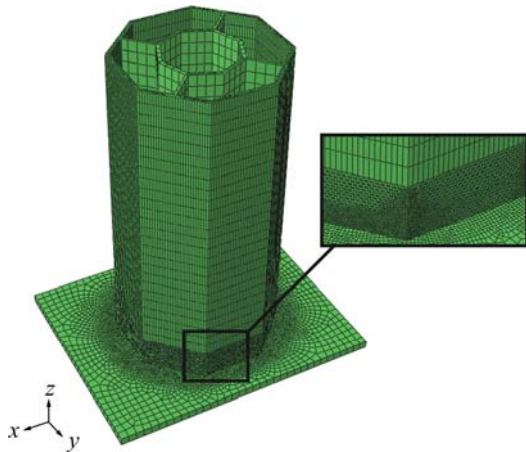


Fig. 2 3D finite element of mesh

partial data of 6061-T6 aluminum alloy. The thermal and mechanical properties of the weld metal and heat-affected zone are the same as the base metal, and the yield behaviour of the welded materials satisfies the von Mises principle [14].

2.3 Welding sequences

A total of nine different welding sequences are studied in the octagonal pipe–plate structure, as shown in Fig. 3, where the black dots denote the welding start

while the arrows represent the welding directions. The case entitled ‘1-seg’ represents that the weld is conducted entirely in one segment from the start to the stop location.

2.4 Thermo-mechanical analysis

Most researchers had studied the thermo-mechanical behaviour in welding simulation using a sequentially coupled formulation [15–19], and therefore some simplifications and approximations were used in their analysis. The direct-coupled method presented in this work is close to the actual welding process in the condition of high nonlinearity. Because of the high thermal conductivity and heat loss of aluminum alloy, a moving ellipsoidal heat source is adopted in the simulation. And it can be described by the following equation:

$$q(x,y,z,t) = \frac{6\sqrt{3}Q}{\pi abc\sqrt{\pi}} \exp\left(\frac{-x^2}{a^2}\right) \exp\left(\frac{-3y^2}{b^2}\right) \exp\left(\frac{-3[z+v(\partial-t)]^2}{c^2}\right) \tag{1}$$

where  $v$  is the welding speed;  $a$ ,  $b$  and  $c$  represent the dimensions of the heat source, and their values are 0.0019 m, 0.0032 m and 0.0028 m, respectively;  $\partial$  is the

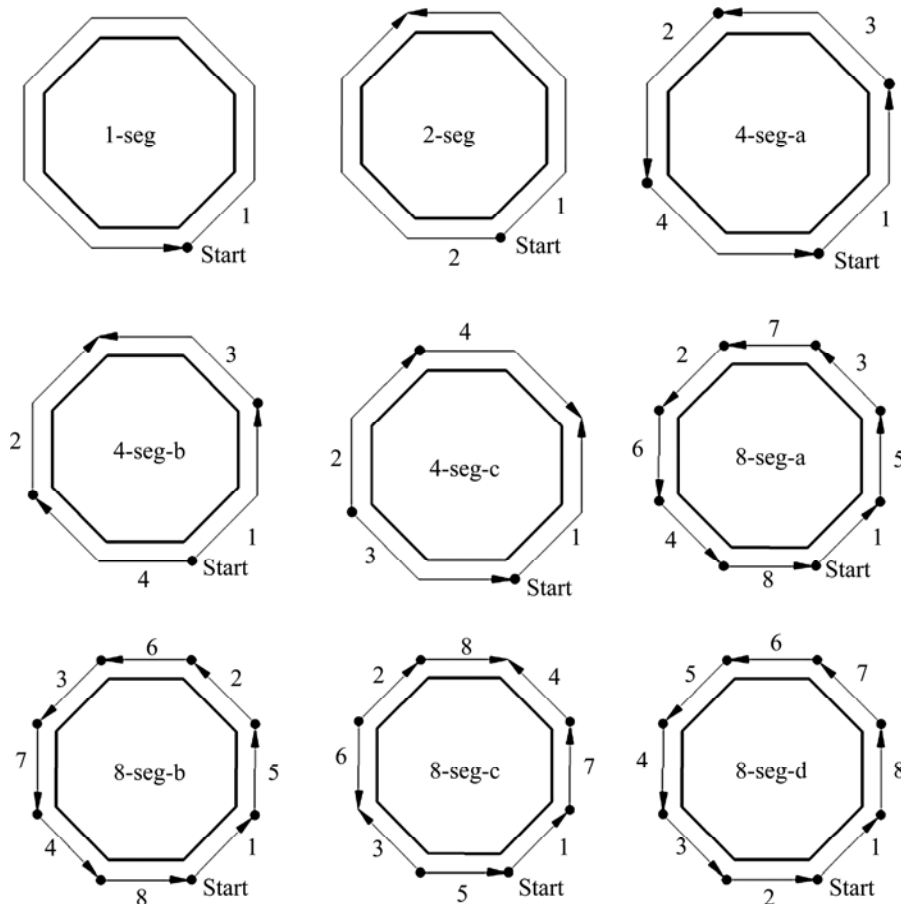


Fig. 3 Nine welding sequences for octagonal pipe-plate weld

time lag of the welding heat source;  $Q$  is the magnitude of the heat input from the welding arc:

$$Q = \eta UI \quad (2)$$

where  $U$  is the welding voltage;  $I$  is the welding current;  $\eta$  represents the thermal efficiency and is assumed to be 0.68 in this study.

To account for heat loss, both thermal radiation and convection are considered and their combined effect, called convective heat transfer coefficient, is presented in the following equation:

$$h = \frac{\varepsilon\sigma[(T + 273)^4 - (T_0 + 273)^4]}{T - T_0} + h_c \quad (3)$$

where  $T_0 = 293$  K represents the room temperature,  $\sigma = 5.67 \times 10^{-8}$  J/(m<sup>2</sup>·K<sup>4</sup>·s) is defined as the Stefan–Boltzmann constant;  $h_c$  is the convective heat coefficient and is estimated to be 15 W/(m<sup>2</sup>·K);  $\varepsilon$  is the emissivity and is set as  $\varepsilon = 0.75$  in the present study.

Since the thermal analysis and mechanical analysis are carried out simultaneously by the direct-coupled method, the FE model used in the mechanical analysis is the same as that used for the thermal analysis. And in the same way, the thermo-mechanical coupling element type, called coupled temp-displacement element in ABAQUS, is used all along. The stress–strain relationship of the welded material is assumed to obey the isotropic Hooke's law. Phase transformation effects are not considered in the study due to lack of material data and the insignificant effect on the welding residual stress.

### 3 Experimental verification

In order to confirm the accuracy of the FE results, a mock up was fabricated with single-pass TIG welding as shown in Fig. 1. The pipe–plate joint was clamped on the plate at the bottom in the welding process. The welding speed, welding voltage and current were 180 mm/min, 10 V and 100 A, respectively.

The distribution of the residual stresses was measured by X-ray diffraction technique using the non-destructive residual stress measurement system (Proto Company, Canada). The longitudinal residual stresses and transverse residual stresses in the vicinity of a welding seam were detected and the measured locations are shown in Fig. 1. The simulation results were compared with the experimental data in Fig. 4. In Fig. 4, the solid curves represent the simulation results while the black triangles are the experimental value.

It can be seen that in the weld and its vicinity, both the longitudinal and transverse residual stress distributions computed by the FE model show good agreement with the experimental data. However, the residual stresses determined by the experiment are higher than the simulated results in a further distance (beyond

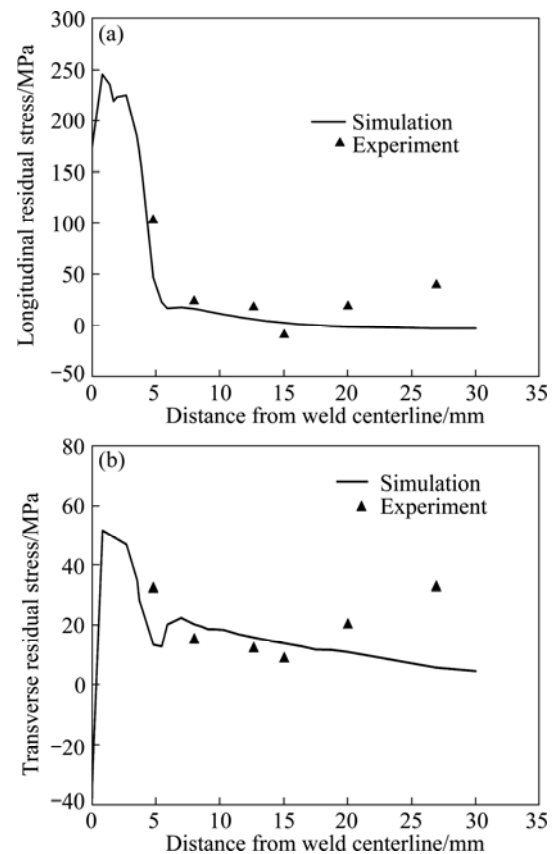


**Fig. 4** Comparison of FEM and experimental results on outer surface of front sections: (a) Longitudinal residual stress; (b) Transverse residual stress

20 mm). This is mainly caused by the previous processing technology. Inevitable residual stresses occur within the pipe after machining process, and this part of residual stresses account for the majority of the final residual stresses. Because the fusion zone and its vicinity are heated up to a high temperature during the welding process, the materials are softened enough and the initial machining residual stresses are cancelled completely [20]. According to Fig. 4, due to a large amount of heat loss of the two points away from the weld, the initial residual stresses are more difficult to cancel by the welding process, so the final residual stresses are mainly determined by machining residual stress. The superposition of the processing technology and the welding effect produce a difference between the simulation results and the experimental values.

## 4 Results and discussion

### 4.1 Residual stress distribution

Residual stress analysis has been run for the 1-seg model, in the four sections of the front, back, left and right around the pipe. Variations of longitudinal residual stress at locations perpendicular to the weld centerline on both outer and inner surfaces are shown in Fig. 5.

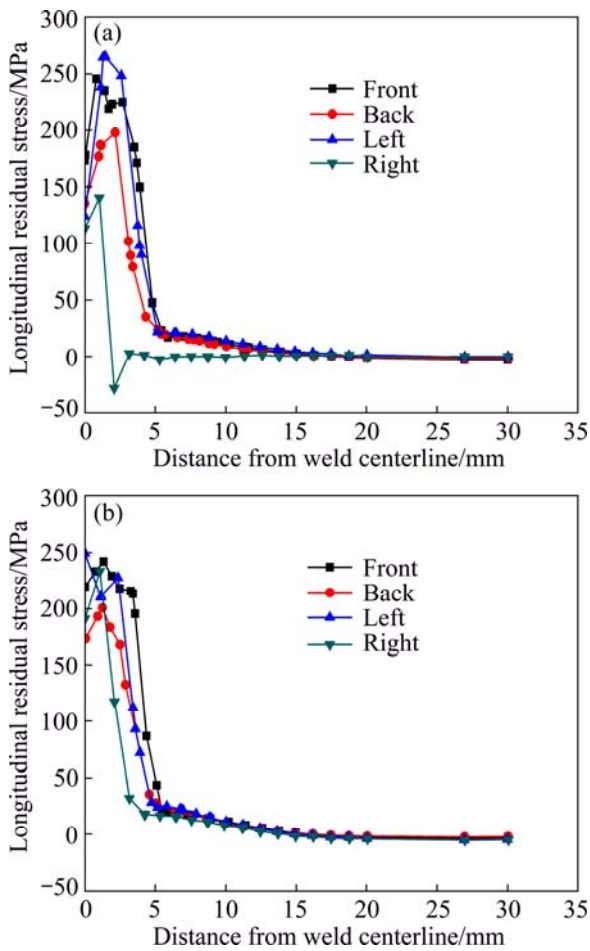


**Fig. 5** Longitudinal residual stresses at locations of different sections for 1-seg model: (a) Outer surface; (b) Inner surface

It can be observed from Fig. 5 that the longitudinal residual stresses are tensile both on the outer and inner surfaces. This is because the thickness of the pipe is quite small and the heat distribution is not much different through the thickness, and the values of longitudinal residual stresses on the outer and inner surfaces are approximately identical. Meanwhile, the shapes of the two longitudinal residual stress curves also show uniformly on both outer and inner surfaces of the pipe.

Figure 6 presents the transverse residual stress distribution in the four sections on both outer and inner surfaces. There are some differences compared with general conditions that axial residual stresses are tensile on the inner surface and compressive on the outer surface within and near the weld in pipe-pipe joint [9]. In pipe-pipe joint, the circumferential shrinkage after welding causes a local inward deformation in the weld and its vicinity, and therefore the axial residual stresses are of a simple linear bending nature. But in the present study, the linear bending after welding is restricted by the plate.

Figure 6 indicates that the magnitude of the transverse residual stress is influenced by the

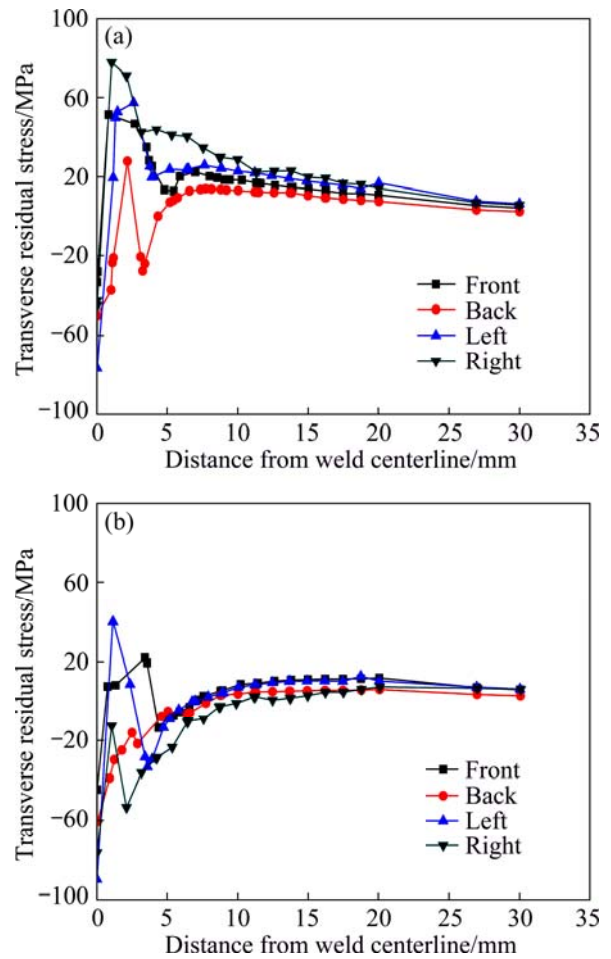


**Fig. 6** Transverse residual stresses at locations of different sections for 1-seg model: (a) Outer surface; (b) Inner surface

longitudinal residual stresses. The residual stresses on both outer and inner surfaces are compressive in the welding seam but tensile nearby, and there is a rapid transition between the residual compressive and tensile stress values in a short distance. Furthermore, like the preceding longitudinal residual stresses, the shapes of the two transverse residual stress curves also show uniformly on both outer and inner surfaces of the pipe.

#### 4.2 Finding the best sequence

The FE model used for the investigation of all nine sequences is shown in Fig. 3. Residual stresses at the end of the final welding sequence are compared to find the optimal welding sequence, and we should first determine which criterion is of the most interest. Since the maximum residual stress is longitudinal residual tensile stress, the longitudinal residual stresses are considered to have the greatest influence on the structural integrity of the weldment. Figure 7 illustrates the longitudinal residual stresses on both outer and inner surfaces.

In the actual working environment, the outer surface is exposed to a more severe environment than the inner

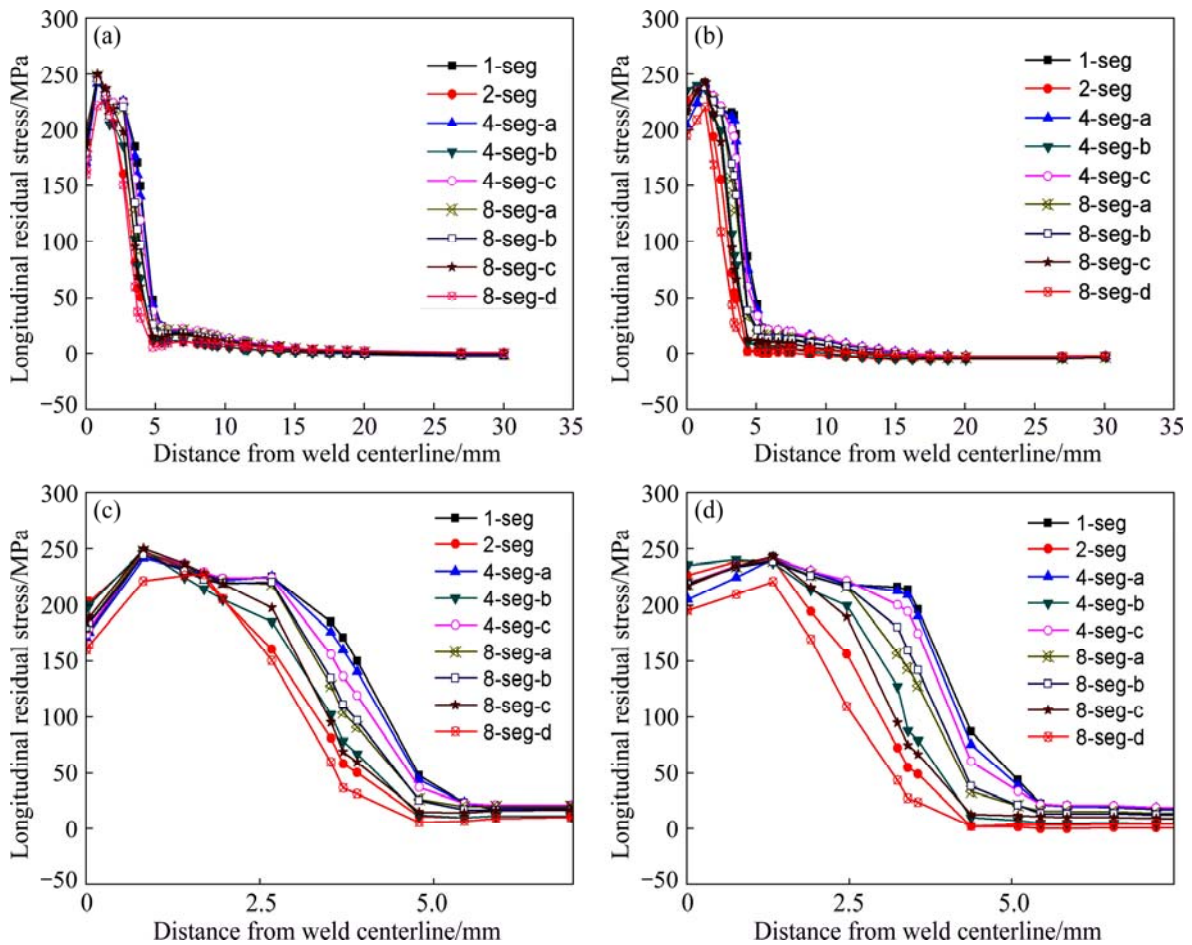


**Fig. 7** Comparison of longitudinal residual stresses of nine sequences in front sections: (a) Outer surface; (b) Inner surface; (c) Magnification of curves within weld zone in Fig. 7(a); (d) Magnification of curves within weld zone in Fig. 7(b)

surface because the outer surface is fully exposed to the air while the inner surface is located in a confined space. Therefore, there exists a risk of stress corrosion cracking because of the high tensile residual stress on the outer surface, and so the longitudinal residual tensile stresses are of the most interest to find the optimal sequence. It can be seen from Fig. 7 that the peak value of the longitudinal residual stress seems not to be affected by the welding sequence, but the magnitude of the longitudinal residual stresses near the weld seam is influenced by different welding sequences. The results are similar to the study conducted by JIANG and YAHIAOUI [21]. They suggested that welding sequences have less effect on the maximum residual stress in the welded piping branch junction. From Fig. 7(c), it can be clearly seen that procedure 8-seg-d produces the lowest longitudinal residual stress in the weld and its vicinity on the outer surface. This might be attributed to the reason that the backstep welding sequence has preheating and post-weld heat treatment effects. Thus, 8-seg-d is the best welding sequence in this study. Furthermore, the sequence of 2-seg also produces

a lower longitudinal residual stress compared with other sequences, largely due to the reduction of the residual shrinkage and stress in the symmetric welding sequence. The worst choice for a welding sequence is 1-seg in this study, and it can be concluded from Fig. 7 that the values of the longitudinal residual stresses on both outer and inner surfaces are not large compared with 1-seg model, which means that increasing the number of sequences in welding process leads to partially decreasing welding residual stress, but this is not absolute as the results shown in the figures. Welding according to 4-seg-a or 4-seg-c produces more longitudinal residual tensile stresses than welding according to 8-seg-a, 8-seg-b or 8-seg-c. Similarly, for symmetric welding sequences, 4-seg-b and 4-seg-c produce higher longitudinal residual stresses than the sequence of 2-seg.

Nine simulation results for transverse residual stress in the front section of the pipes on both outer and inner surfaces are compared in Fig. 8. On the outer surface, the shape of the transverse residual stress curves under different welding sequences shows uniformly, and the variation of the transverse residual stresses near the weld

seam due to different welding sequences is not large. But the distribution of the transverse residual stresses on the inner surface of the pipe is affected by welding sequence. This may be caused by the uneven heat distribution on the outer and inner surfaces during welding process. Like the preceding longitudinal residual stress, the welding sequences have little effect on the transverse residual stress distribution at parts away from the weld zone.

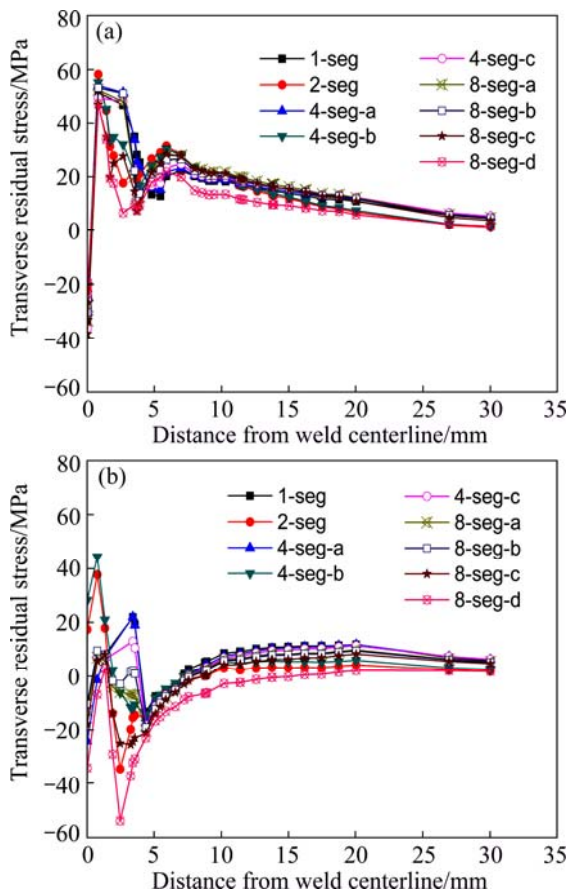


**Fig. 8** Comparison of transverse residual stresses of nine sequences in front sections: (a) Outer surface; (b) Inner surface

## 5 Conclusions

1) The final residual stresses in the weld and its vicinity are not affected by the initial residual stresses and only determined by the welding process, while the initial residual stresses account for the majority of the final residual stresses away from the weld.

2) Simulation results show that in thin-walled single-pass welding of octagonal pipe-plate joint, the longitudinal residual stresses are tensile both on the outer and inner surfaces in the weld and its vicinity. While there is a rapid transition from compressive to tensile for the transverse residual stresses within the weld zone.

3) Increasing the number of welding sequences does not always lead to decreasing welding residual stresses in polygonal pipes.

4) The distribution of the residual stresses is affected by welding sequence and reasonable welding sequences can effectively reduce the residual stresses in regular octagonal pipe-plate joint. In the present analysis, backstep welding is the optimal welding sequence and symmetric welding is also an available welding sequence.

## References

- [1] LIU C, ZHANG J X, XUE C B. Numerical investigation on residual stress distribution and evolution during multipass narrow gap welding of thick-walled stainless steel pipes [J]. *Fusion Engineering and Design*, 2011, 86: 288–295.
- [2] SCHENK T, RICHARDSON I M, KRASKA M, OHNIMUS S. A study on the influence of clamping on welding distortion [J]. *Computational Materials Science*, 2009, 45: 999–1005.
- [3] JIANG W C, ZHANG Y C, WOO W C. Using heat sink technology to decrease residual stress in 316L stainless steel welding joint: Finite element simulation [J]. *International Journal of Pressure Vessels and Piping*, 2012, 92: 56–62.
- [4] TENG T L, CHANG P H, TSENG W C. Effect of welding sequences on residual stresses [J]. *Computers & Structures*, 2003, 81: 273–286.
- [5] GUIRAO J, RODRÍGUEZ E, BAYÓN A, BOUYER F, PISTONO J, JONES L. Determination through the distortions analysis of the best welding sequence in longitudinal welds VATS electron beam welding FE simulation [J]. *Fusion Engineering and Design*, 2010, 85: 766–779.
- [6] GANNON L, LIU Y, PEGG N, SMITH M. Effect of welding sequence on residual stress and distortion in flat-bar stiffened plates [J]. *Marine Structures*, 2010, 23: 385–404.
- [7] JIANG W, YAHIAOUI K. Effect of welding sequence on residual stress distribution in a multipass welded piping branch junction [J]. *International Journal of Pressure Vessels and Piping*, 2012, 95: 39–47.
- [8] ZENG Z, WANG L J, DU P G, LI X B. Determination of welding stress and distortion in discontinuous welding by means of numerical simulation and comparison with experimental measurements [J]. *Computational Materials Science*, 2010, 49: 535–543.
- [9] CHANG K H, LEE C H. Effect of the welding sequence in the circumferential direction on residual stress distribution in a thin-walled pipe weld [J]. *Proceedings of the Institution of Mechanical Engineers, Part B: Journal of Engineering Manufacture*, 2009, 223: 723–735.
- [10] SATTARI-FAR I, JAVADI Y. Influence of welding sequence on welding distortions in pipes [J]. *International Journal of Pressure Vessels and Piping*, 2008, 85: 265–274.
- [11] HACKMAIR C, WERNER E, PÖNISCH M. Application of welding simulation for chassis components within the development of manufacturing methods [J]. *Computational Materials Science*, 2003, 28: 540–547.
- [12] DENG D A. FEM prediction of welding residual stress and distortion in carbon steel considering phase transformation effects [J]. *Materials & Design*, 2009, 30: 359–366.
- [13] YAGHI A, HYDE T H, BECKER A A, SUN W, WILLIAMS J A. Residual stress simulation in thin and thick-walled stainless steel pipe welds including pipe diameter effects [J]. *International Journal of Pressure Vessels and Piping*, 2006, 83: 864–874.
- [14] JI S D, FANG H Y, LIU X S, MENG Q G. Influence of a welding sequence on the welding residual stress of a thick plate [J]. *Modelling and Simulation in Materials Science and Engineering*, 2005, 13: 553–565.

- [15] DENG D A, KIYOSHIMA S. FEM prediction of welding residual stresses in a SUS304 girth-welded pipe with emphasis on stress distribution near weld start/end location [J]. Computational Materials Science, 2010, 50: 612–621.
- [16] ANCA A, CARDONA A, RISSO J, FACHINOTTI V D. Finite element modeling of welding processes [J]. Applied Mathematical Modelling, 2011, 35: 688–707.
- [17] OGAWA K, DENG D A, KIYOSHIMA S, YANAGIDA N, SAITO K. Investigations on welding residual stresses in penetration nozzles by means of 3D thermal elastic plastic FEM and experiment [J]. Computational Materials Science, 2009, 45: 1031–1042.
- [18] DENG D A, MURAKAWA H, LIANG W. Numerical simulation of welding distortion in large structures [J]. Computer Methods in Applied Mechanics and Engineering, 2007, 196: 4613–4627.
- [19] YAN D Y, WU A P, SILVANUS J, SHI Q Y. Predicting residual distortion of aluminum alloy stiffened sheet after friction stir welding by numerical simulation [J]. Materials & Design, 2011, 32: 2284–2291.
- [20] DENG D A, KIYOSHIMA S. Numerical simulation of residual stresses induced by laser beam welding in a SUS316 stainless steel pipe with considering initial residual stress influences [J]. Nuclear Engineering and Design, 2010, 240: 688–696.
- [21] JIANG W, YAHIAOUI K. Effect of welding sequence on residual stress distribution in a multipass welded piping branch junction [J]. International Journal of Pressure Vessels and Piping, 2012, 95: 39–47.

## 焊接顺序对薄壁八边形管-板焊接接头 残余应力的影响

傅定发<sup>1</sup>, 周长青<sup>1</sup>, 李 灿<sup>1</sup>, 王 冠<sup>2</sup>, 李落星<sup>2</sup>

1. 湖南大学 材料科学与工程学院, 长沙 410082;

2. 湖南大学 汽车车身先进设计与制造国家重点实验室, 长沙 410082

**摘 要:** 考虑实际焊接中热-机械的直接耦合效应, 通过热-弹塑性有限元法建立三维有限元模型来研究不同焊接顺序对薄壁 6061 铝合金焊件焊后残余应力分布的影响, 采用单道 TIG 焊接实验来验证模拟结果的准确性; 利用九种不同的焊接顺序来研究八边形管和底板之间焊后残余应力的分布状态。结果表明, 焊缝及其附近存在的初始残余应力并不影响最终残余应力的分布; 选择合理的焊接顺序可以有效降低八边形管-板接头的残余应力。

**关键词:** 残余应力; 焊接顺序; 管-板接头; 单道焊接; 初始残余应力

(Edited by Hua YANG)